Scientia Iranica B (2017) 24(1), 223–236

SCIENTIA IRANICA

Sharif University of Technology
Scientia Iranica
Transactions B: Mechanical Engineering
www.scientiairanica.com

Numerical assessment of turbulence effects on forces, spray parameters, and secondary impact in wedge water entry problem using $k-\varepsilon$ method

R. Shademani and P. Ghadimi*

Department of Marine Technology, Amirkabir University of Technology, Tehran, P.O. Box 15875-4413, Iran.

Received 12 May 2015; received in revised form 12 February 2016; accepted 10 May 2016

KEYWORDS
Wedge water entry;
Free surface;
Impact force;
Secondary impact;
Finite volume method;
Volume of fluid.

Abstract. The present paper focuses on the assessment of turbulence effects on the impact force, spray, and secondary impact force of the wedge water entry. For this purpose, a finite element-based finite volume method code coupled with volume of fluid has been developed. The $k-\varepsilon$ method has also been implemented to model the turbulence effects. The developed code is validated against experimental data with good accordance and is then used to model the water entry of wedges with deadrise angles ranging from 10 to 60 degrees at different velocities of 1 and 2 m/s with laminar and turbulent assumptions. Subsequently, the resulting forces and free surfaces are compared for three critical instances of "peak", "hollow", and "2nd impact". It is illustrated that turbulence has negligible effects on the force and free surface in the main water entry process. However, turbulent effects rise up to 14.23% for the secondary impact forces.

1. Introduction

The water entry problem has been numerically and analytically investigated by many researchers using various methodologies through applying different assumptions on the physics of the flow. However, there are still uncertainties about some of these assumptions and their effects on the results. Accordingly, there are choices to be made prior to the solution of the problem, which are still unclear.

One of these assumptions is the choice between turbulent and laminar flows. Turbulence can be described as the chaotic behavior of the fluid. Although there is not a clear definition of "turbulence", the common aim of different turbulence theories is to describe these random behaviors as formulated fluctuations in the fluid properties. These models are mainly extracted either by imposing different assumptions on the fluid or by the use of relations deduced from the experiments. Therefore, using turbulence models does not necessarily guarantee better results in many situations. Indeed, one of the ambiguities concerning the flow around wedges in the water entry problem is whether it should be assumed laminar or turbulent.

Before addressing this question, which is the main concern of the present manuscript, a literature review of different works on the simulation of water entry problem in recent years is presented to highlight the importance of this problem in the scientific community.

Water entry of wedges has been simulated using many different numerical methods. Luo et al. [1] used Finite Element Method (FEM) to solve this problem with a laminar assumption. Yang and Qiu [2] also assumed a laminar flow and used Finite difference method to solve the water entry problem. The newly introduced Smoothed Particle Hydrodynamics method

*. *Corresponding author. Tel.: +98 21 64543110; Fax: +98 21 66412495*
E-mail address: pghadimi@aut.ac.ir (P. Ghadimi)

(SPH) has also been used in the recent years [3-6] to study this problem. However, it has mainly been used in conjunction with a turbulence theory. Moreover, Wang and Wei [7], Yin and Qian [8], and Sun et al. [9] used Boundary Element method to solve the water entry problem by using potential theory, which basically neglects the viscosity effects and hence the turbulence effects. On the other hand, analytical method has been used by Ghadimi et al. [10] by applying the Schwartz-Christoffel conformal mapping, a solution which neglects viscosity effects. The works by Gao et al. [11] and Wu et al. [12] are other studies, which have used potential theory to solve the wedge water entry problem. Other researchers who chose laminar assumptions include Khabakhpasheva and Korobkin [13], Yamada et al. [14], Alaoui and Neme [15], and Luo et al. [16]. On the other hand, other researchers who have conducted a turbulent simulation include Yang et al [17-19], Feizi Chekab et al. [20], Ghadimi et al. [21,22], Farsi and Ghadimi [23-25], and Viviani et al. [6].

As extracted from the literature, the best choice between laminar and turbulent simulations is not so clear. Accordingly, the focus of the present paper is to show the differences of the effects of laminar and turbulent assumptions in the water entry problem. To this end, Navier-Stokes equations are solved using finite element-based finite volume method (FEM-FVM) coupled with volume of fluid (VOF) method. To consider the turbulence effect, the $k-\varepsilon$ turbulence model has been implemented in the code. Wedges with deadrises of 10 to 80 degrees have been considered to assess the turbulence effect at extremely low and extremely high deadrise angles. Width of the considered wedges has been assumed constant as a design parameter. Specific parameters are defined for describing and analyzing the spray and cavity formation above the chine for comparison purposes.

In the following sections, after describing the governing equations and discretization methods, validation of the code is presented. Afterward, the comparison of forces, spray parameters, and cavity formation is presented for laminar and turbulent simulations of different wedges.

2. Governing equations

2.1. Momentum equations

Navier Stokes equations are solved for a two-phase flow in a homogeneous mode using finite element-based finite volume method coupled with volume of fluid method. The continuity and conservation of momentum equations can be written as:

$$\frac{\partial \rho}{\partial t}+\frac{\partial \rho u}{\partial x}+\frac{\partial \rho v}{\partial y}=0, \tag{1}$$

$$\frac{\partial \rho \varphi}{\partial t}+\frac{\partial \rho u \varphi}{\partial x}+\frac{\partial \rho v \varphi}{\partial y}=\frac{\partial}{\partial x}\mu\frac{\partial \varphi}{\partial x}+\frac{\partial}{\partial y}\mu\frac{\partial \varphi}{\partial y}+S, \tag{2}$$

where, x and y are the coordinate directions, t is time, ρ is the fluid density, μ is the dynamic viscosity, $S=-\frac{\partial P}{\partial x}+\rho g_x$ and $\varphi=u$ are in the x direction, and $S=-\frac{\partial P}{\partial y}+\rho g_y$ and $\varphi=v$ are in the y direction, in which P is the pressure and u and v are the velocities in the x and y directions, respectively.

2.2. Volume Of Fluid (VOF) method

In the volume of fluid scheme, a scalar parameter named volume fraction (α) is defined as the fraction of an element filled with one fluid. As a result, $(1-\alpha)$ is the fraction of the second fluid. VOF method is based on the conservation of the scalar parameter (α) with respect to time and space, which can be described by the relation:

$$\frac{\partial \alpha}{\partial t}+\nabla.(U\alpha)=0, \tag{3}$$

where U is the fluid velocity vector. By using the volume fraction, an equivalent density and viscosity can be calculated for each element using the equations:

$$\rho_{\text{eq}}=\alpha\rho_1+(1-\alpha)\rho_2,$$

$$\upsilon_{\text{eq}}=\alpha\upsilon_1+(1-\alpha)\upsilon_2, \tag{4}$$

where α is the volume fraction and ρ_1, ρ_2 and υ_1, υ_2 are the density and viscosity of the fluids, while ρ_{eq} and υ_{eq} are the equivalent fluid density and viscosity, respectively.

In the VOF scheme, Eq. (3) is used to move the volume fraction field with the fluid velocities. In this way, the free surface is transferred using the velocity field of both fluids.

In the next section, the applied numerical method is briefly explained.

2.3. Turbulence model

To implement the turbulence effect, the standard $k-\varepsilon$ turbulence model has been used, which is found in most CFD references. The transport equations for k and ε are as follows:

$$\frac{\partial(\rho k)}{\partial t}+\frac{\partial}{\partial x_j}(\rho U_j k)=\frac{\partial}{\partial x_j}\left[\left(\mu+\frac{\mu_t}{\sigma_k}\right)\frac{\partial k}{\partial x_j}\right]+P_k-\rho\varepsilon+P_{kb}, \tag{5}$$

$$\frac{\partial(\rho \varepsilon)}{\partial t}+\frac{\partial}{\partial x_j}(\rho U_j \varepsilon)=\frac{\partial}{\partial x_j}\left[\left(\mu+\frac{\mu_t}{\sigma_\varepsilon}\right)\frac{\partial \varepsilon}{\partial x_j}\right]+\frac{\varepsilon}{k}(C_{\varepsilon 1}P_k-C_{\varepsilon 2}\rho\varepsilon+C_{\varepsilon 1}P_{\varepsilon b}), \tag{6}$$

where μ_t is the turbulent viscosity; P_k is the product of k; P_{kb} and $P_{\varepsilon b}$ are the buoyancy effects; and $C_{\varepsilon 1}$, $C_{\varepsilon 2}$, σ_k, and σ_ε are constants.

2.4. Numerical method

In the finite element-based finite volume method (FEM-FVM), shape functions are defined on each node of the elements as:

$$\varphi = \sum_{i=1}^{\text{Node}} N_i \varphi_i,$$

where N_i is the shape function at node i and φ_i is the quantity of φ at that node. The discretization method adopted in this paper is based on the fully coupled Rhie and Chow [26] algorithm, applied on a collocated triangular grid system for a 2D fluid flow. The shape functions for triangular elements are as follows:

$$N_1 = \left(\frac{y_2 - y_1}{\text{DET}}\right) x + \left(\frac{x_3 - x_2}{\text{DET}}\right) y + \left(\frac{x_2 y_3 - x_3 y_2}{\text{DET}}\right),$$

$$N_2 = \left(\frac{y_3 - y_1}{\text{DET}}\right) x + \left(\frac{x_1 - x_3}{\text{DET}}\right) y + \left(\frac{x_3 y_1 - x_1 y_3}{\text{DET}}\right),$$

$$N_3 = \left(\frac{y_1 - y_2}{\text{DET}}\right) x + \left(\frac{x_2 - x_1}{\text{DET}}\right) y + \left(\frac{x_1 y_2 - x_2 y_1}{\text{DET}}\right),$$

$$\text{DET} = (x_1 y_2 + x_2 y_3 + x_3 y_1 - y_1 x_2 - y_2 x_3 - y_3 x_1), \quad (7)$$

where DET is the determinant of the coordinates matrix and x_i and y_i are the coordinates of the triangle points. By implementing the Navier-Stokes equations in a control volume, the following equation can be obtained:

$$\underbrace{\left(\frac{\partial \rho\varphi}{\partial t}\right)_i \tilde{\forall}_i}_{\text{Transient}} + \underbrace{\rho u \varphi ds_x|_{j,k} + \rho v \varphi ds_y|_{j,k}}_{\text{Convection}} = \underbrace{\mu \overrightarrow{\nabla\varphi}.\overrightarrow{ds}\Big|_{j,k}}_{\text{Diffusion}} + \underbrace{\int_{\tilde{\forall}_i} b d\forall}_{\text{Source}}. \quad (8)$$

The transient terms can be expressed on a control volume ($\tilde{\forall}_i$) as follows:

$$\frac{\partial}{\partial t}\int_{\forall} \rho\varphi d\forall \cong \left(\rho \frac{\partial \varphi_i}{\partial t}\right) \tilde{\forall}_i = \rho \tilde{\forall}_i \frac{\varphi_i - \varphi_i^0}{\Delta t}. \quad (9)$$

The Upwind Difference Scheme (UDS) is used for the convection term on a control line j, k as follows:

$$\int_{S_{j,k}} \rho \vec{V} \varphi ds = (\rho \vec{V}.\overrightarrow{ds})_{j,k} \varphi_{j,k}. \quad (10)$$

The false diffusion problem is eliminated by using the method introduced by Karimian and Schneider [27] as in:

$$\left(\rho \vec{V}.\overrightarrow{ds}\right)_{j,k} \varphi_{j,k} = \left(\rho \overrightarrow{\hat{V}}.\overrightarrow{ds}\right)_{j,k} \varphi_{j,k}, \quad (11)$$

where φ_j is calculated as:

$$\varphi_j = \varphi_{upj} + \frac{\partial \varphi}{\partial s}\Delta s. \quad (12)$$

For the x direction, Eq. (13) is obtained:

$$\hat{u}_j = \frac{(\overline{\rho \bar{v}})_j}{\Delta s_j d} U_{upj} + \frac{\mu}{d d_j^2} \sum_{i=1}^{3} (N_i)_j U_i - \frac{1}{d}\frac{\partial}{\partial x} \sum_{i=1}^{3} (N_i)_j P_j. \quad (13)$$

Here, j is the present node and i is the element node.

Also, pressure and diffusion terms are modeled as follows:

$$\int_{\forall} -\frac{\partial p}{\partial x} d\forall = \int_S -P ds_x,$$

$$\int_{\forall} -\frac{\partial p}{\partial y} d\forall = \int_S -P ds_y, \quad (14)$$

$$-\mu \overrightarrow{\nabla\varphi}.\overrightarrow{ds}\Big|_{j,k} = -\left(\mu \frac{\partial \varphi}{\partial x} ds_x + \mu \frac{\partial \varphi}{\partial y} ds_y\right)\Big|_{j,k}. \quad (15)$$

The developed code is based on the global algorithm displayed in Figure 1.

By using the algorithm displayed in Figure 1, a computer code has been developed for solving the wedge water entry problem. In the next sections, after validating the code, the laminar and turbulent water entry problems of different wedges are analyzed and compared.

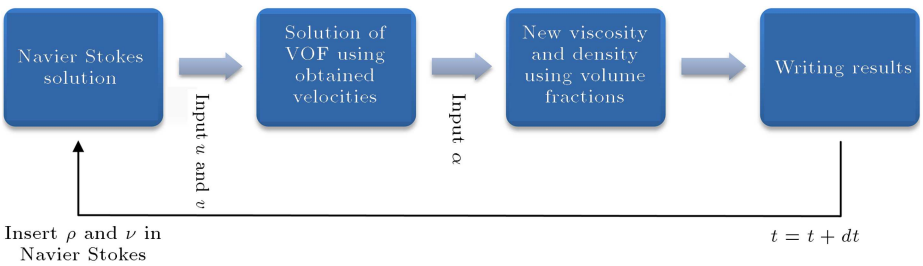

Figure 1. Numerical algorithm.

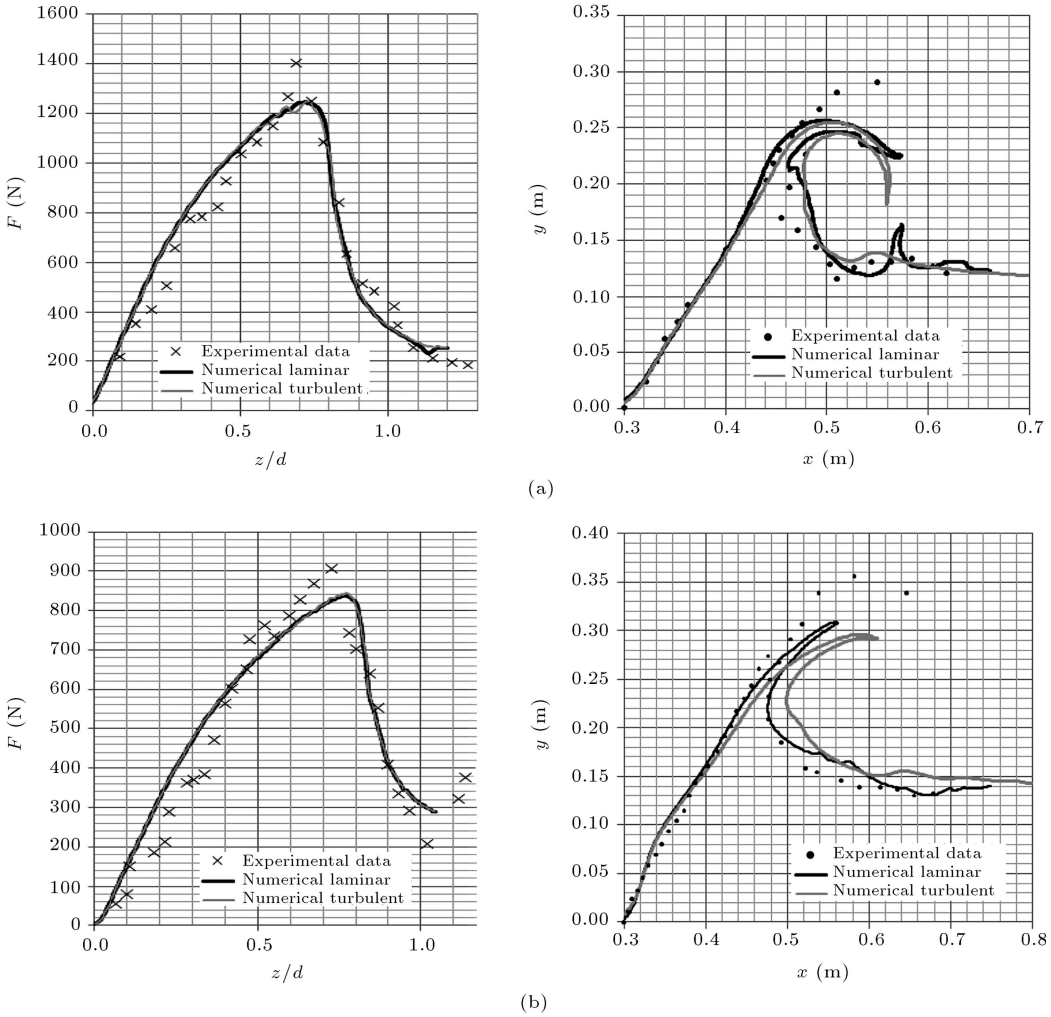

Figure 2. Water entry forces (left) and free surface (right): Comparison of laminar and turbulent numerical results versus experimental data [28] for (a) 10 degrees and (b) 15 degrees of deadrise angle.

2.5. Wedge force calculation

One of the most important outputs of the present study is the force acting on the wedge while entering the water. The force acting on the wedge is due to pressure and shear stress, which are calculated by the following equations:

$$F_n = F_{\text{pressure}} = \int_{\text{Wedge.surface}} PdA, \tag{16}$$

$$F_t = F_{\text{shear.stress}} = \int_{\text{Wedge.surface}} \tau dA, \tag{17}$$

where F_n is the force normal to the wedge, F_t is the force tangential to the wedge, and τ is the shear stress. The vertical impact force (F) is calculated using the relation:

$$F = F_n \cos\theta + F_t \sin\theta, \tag{18}$$

where θ is the angle of the wedge surface with the horizon.

3. Validation

To validate the developed code, experimental results of Tveitnes et al. [28] have been utilized. Water entries of two wedges with 10 and 15 degrees of deadrise angle have been simulated at an entry speed of 0.94 m/s and the results are illustrated in Figure 2.

As observed in Figure 2, there are reasonable errors of 5.36% and 7.48% for the wedges of 10 degrees and 15 degrees, respectively. Also, by comparing the numerically obtained free surface against the plots provided by Tveitnes et al. [28], it is demonstrated that there is good similarity between the numerical and experimental free surfaces.

The local Reynolds number of the flow near the wedge reaches 5.5×10^6, which is in the range of turbulence. However, the question is how much the turbulence assumptions may affect the flow analysis for the wedge water entry and under what circumstances the turbulence effects could be neglected. As a preliminary comparison between laminar and turbulent results, it is

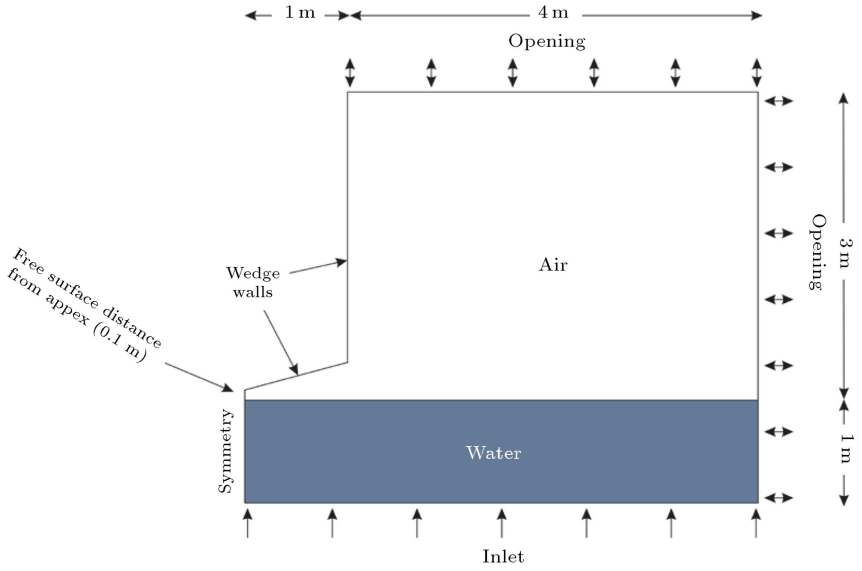

Figure 3. Numerical domain and boundary conditions illustrated in a sample mesh of the problem.

clear that there is no difference in the force estimation. However, there are slight differences in the free surfaces. To better diagnose the effect of turbulence in the water entry problem, more tests at different deadrise angles are conducted in the next section.

4. Results and discussion

As pointed out earlier, the present study is focused on the effects of turbulent and laminar assumptions on the impact force, the secondary impact force, and the free surface of the water entry problem. To this end, the problem should be solved for a wide range of deadrises with laminar and turbulent assumptions. In this section, the flow characteristics for wedges with 10, 15, 20, 30, 40, 50, and 60 degrees of deadrise angles are presented. The numerical setup shown in a sample mesh of the problem is illustrated in Figure 3.

As observed in Figure 3, because of the symmetric nature of the problem, half of the wedge has been modeled and a symmetry boundary condition has been applied. The wedge is modeled as a no-slip wall. An initial distance of 0.1 m has been taken into account to better capture the impact. The water is injected to the domain from the bottom to raise the water surface level and simulate downward motion of the wedge. Also, a hexagonal mesh has been applied and it is tried to obtain the highest possible orthogonality.

The typical impact force versus time is presented in Figure 4.

As shown in Figure 4, there are 3 critical points in the water entry impact force versus time, which are hereafter named "peak", "hollow", and "2nd Impact". At each point, the force and free surface for all deadrise angles at two entry velocities are extracted

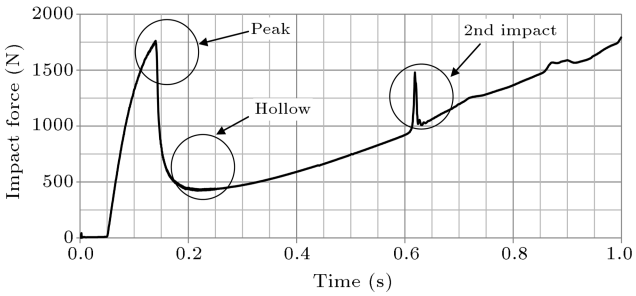

Figure 4. Definition of the critical moments for comparison of force and free surface.

and overlaid for comparing the laminar and turbulent solutions. Typically extracted figures are presented in Figure 5 for one particular deadrise angle and velocity.

The obtained impact forces versus time for different deadrise angles are presented in Figuew 6. As observed in Figure 6, there is hardly any difference between laminar and turbulent simulations and the turbulence effects may be neglected.

In the following subsections, the forces and free surfaces in these three critical times are presented and the difference between laminar and turbulent solutions is examined.

4.1. Turbulent versus laminar at "peak" point

When plotting the trend of impact force over time, it is observed that the impact force grows while the spray root ascends along the wedge. When the spray root arrives at the chine, the impact force rapidly diminishes and the "peak" point occurs. The "peak" impact force is presented in Figure 7.

As observed in Figure 7, there is no significant difference between the peak forces in laminar and turbulent simulations in most cases. The highest

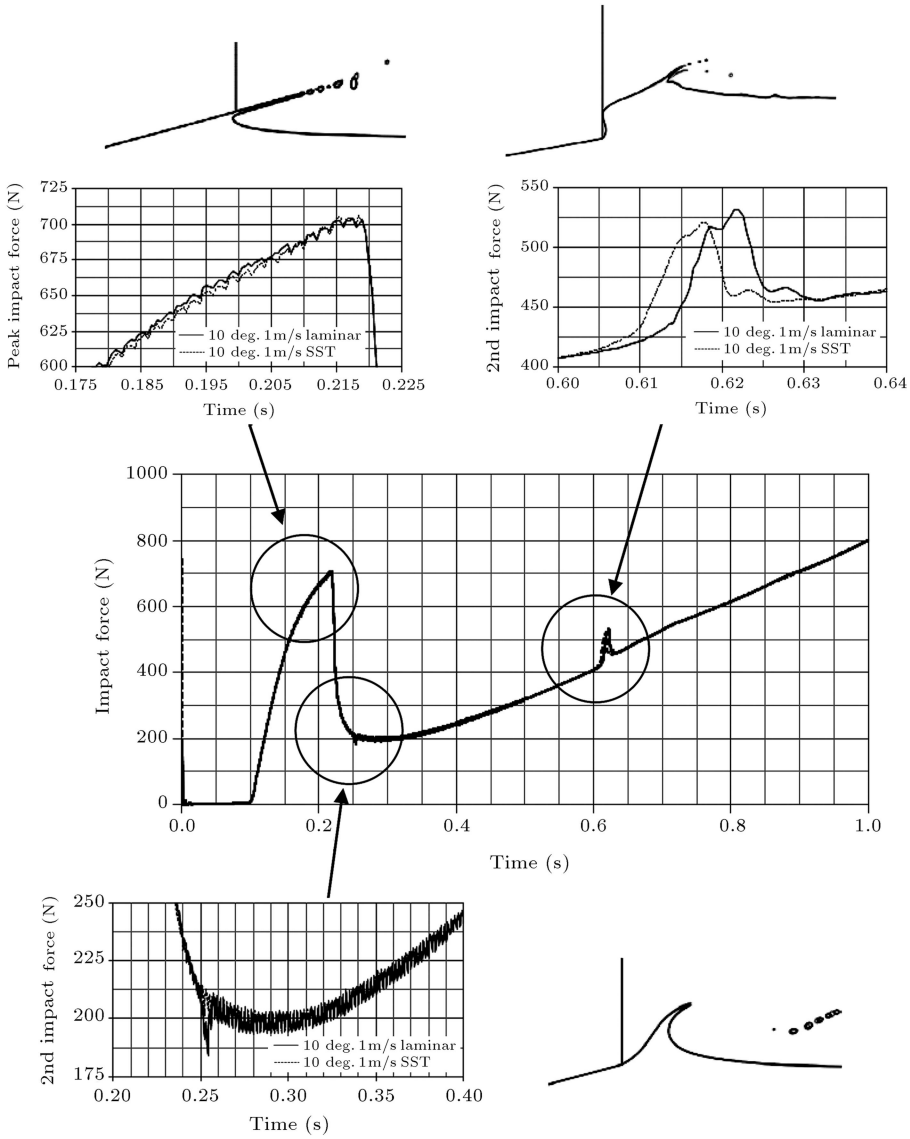

Figure 5. Schematic of the relation between peak, hollow, and 2nd impact and the free surface.

difference is 1.33%, which occurs at 30 degrees. and 2 m/s, and can generally be neglected in most of the engineering analyses.

Meanwhile, the free surfaces related to the "peak" condition are illustrated in Figure 8.

It is quite evident in Figure 8 that there is very little difference between the free surfaces. It is hard to find a well defined difference basis for the free surface, due to the fact that the shapes of the free surfaces are almost similar in all cases for the laminar and turbulent simulations. However, it could be mentioned that there are negligible deviations in the direction of the water jet.

4.2. Turbulent versus Laminar in "hollow" point

After the "peak" condition, the impact force decreases rapidly to the lowest level and then increases again, forming a "hollow" point in the impact force diagram. This occurs simultaneously with the spray detachment from the chine. The forces at the "hollow" point are depicted in Figure 9.

As observed in Figure 9, the impact force is oscillatory in this region for most of the considered cases. However, it can be claimed that the difference between the mean impact forces is negligible, where the maximum deviation is about 2.77%, which occurs at 15 degrees and 2 m/s; again, a difference which can be neglected.

The free surfaces related to the hollow point for the turbulent and laminar flows are presented in Figure 10.

It can be deduced from the free surfaces depicted in Figure 10 that, again, although there are slight differences in the directions of the spray, the overall differences in the free surfaces are negligible.

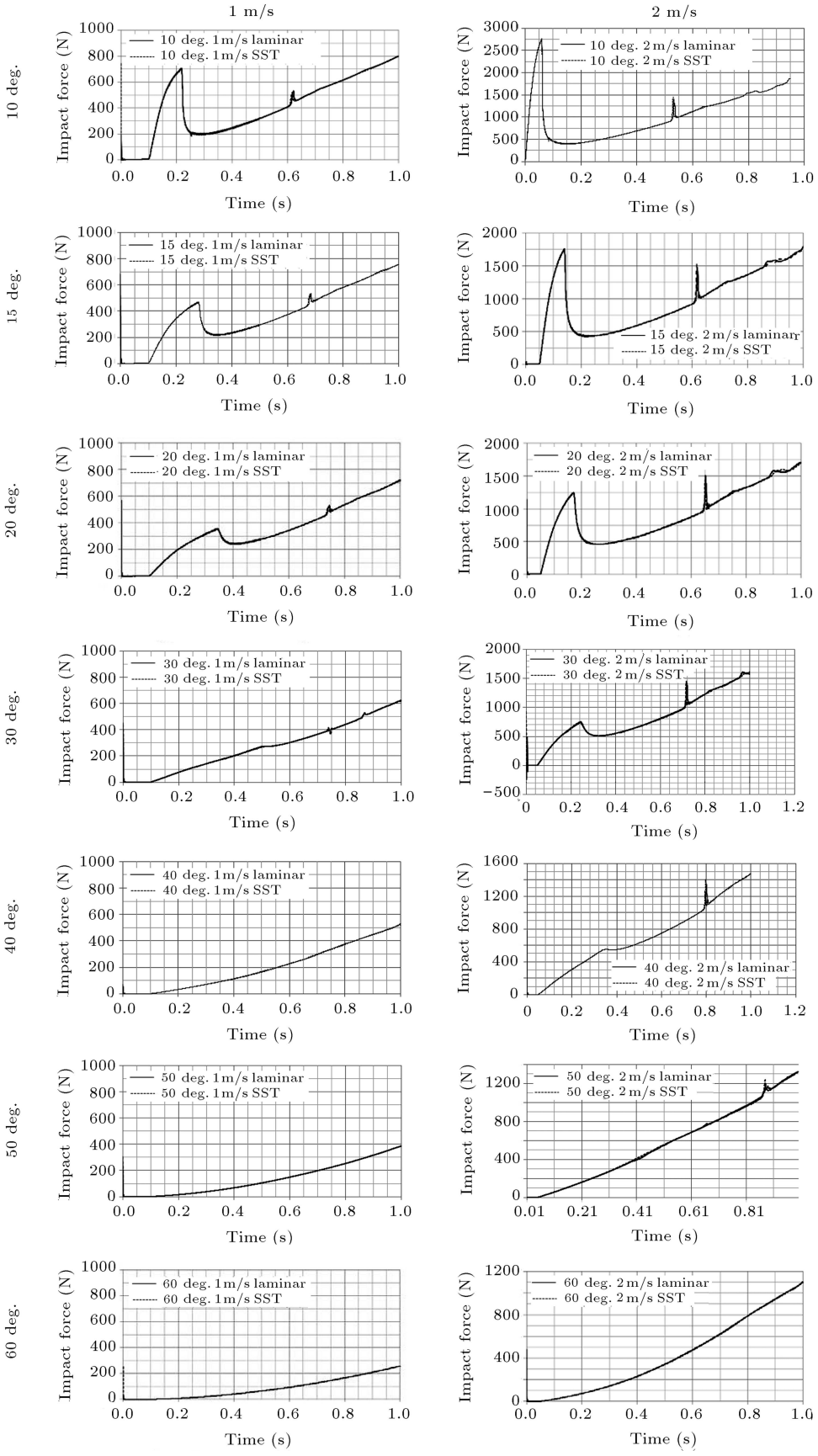

Figure 6. Vertical impact forces acting on the wedges of different deadrises at different entry speeds in turbulent and laminar simulations.

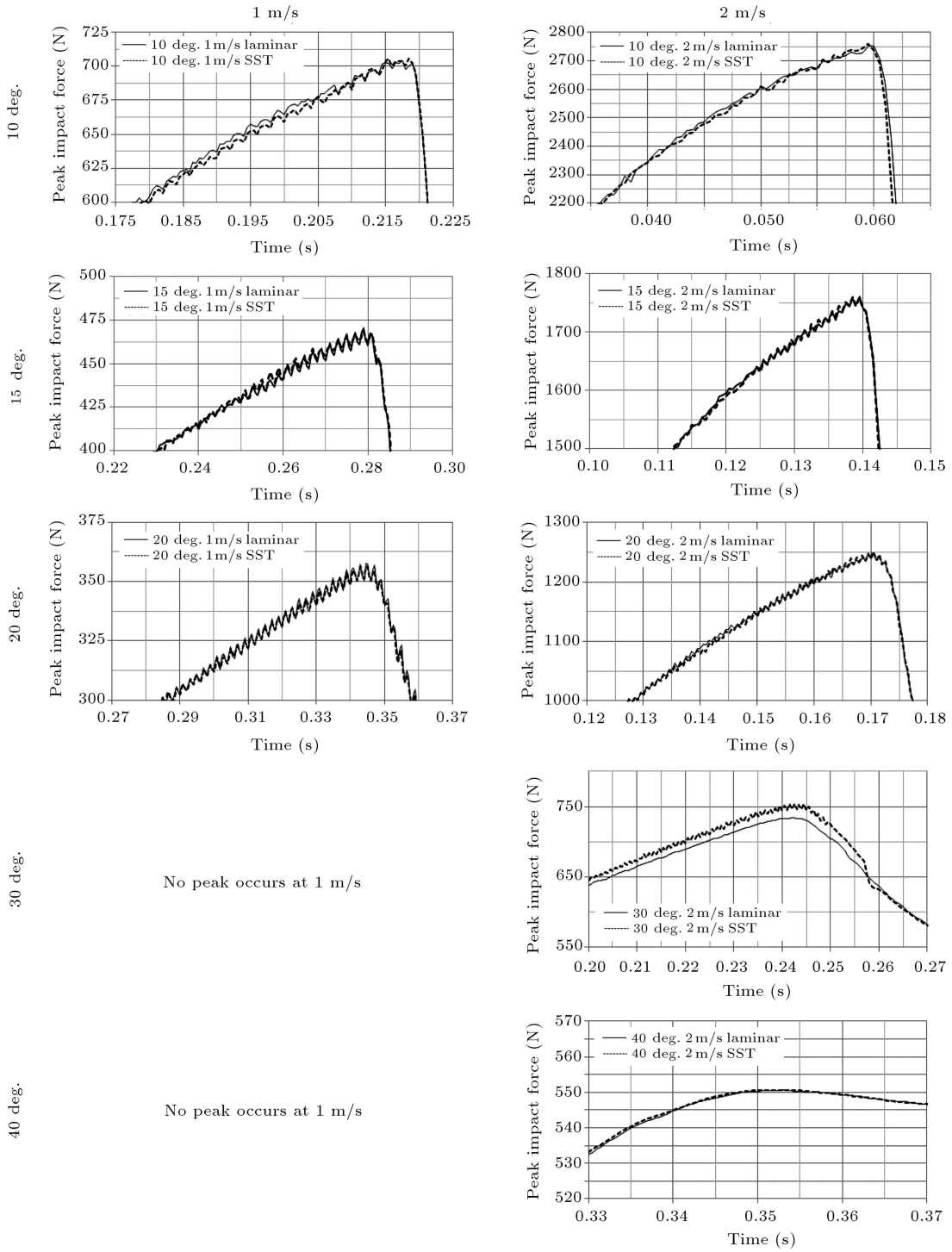

Figure 7. Hollow impact forces acting on the wedges of different deadrise angles at different speeds in turbulent and laminar simulations.

4.3. Turbulent versus laminar in "2nd impact" point

After the detachment of the spray from the chine, an empty region is formed above the chine, which causes the water to return to the wedge, resulting in a secondary impact on the wedge wall above the chine. This process is displayed in Figure 11.

The secondary impact gives birth to an air cavity above the chine, which is important in some applications even at low speeds.

The impact force for the "2nd impact" point is presented in Figure 12.

It is clearly shown in the 2nd impact forces displayed in Figure 12 that there is a time shift in the

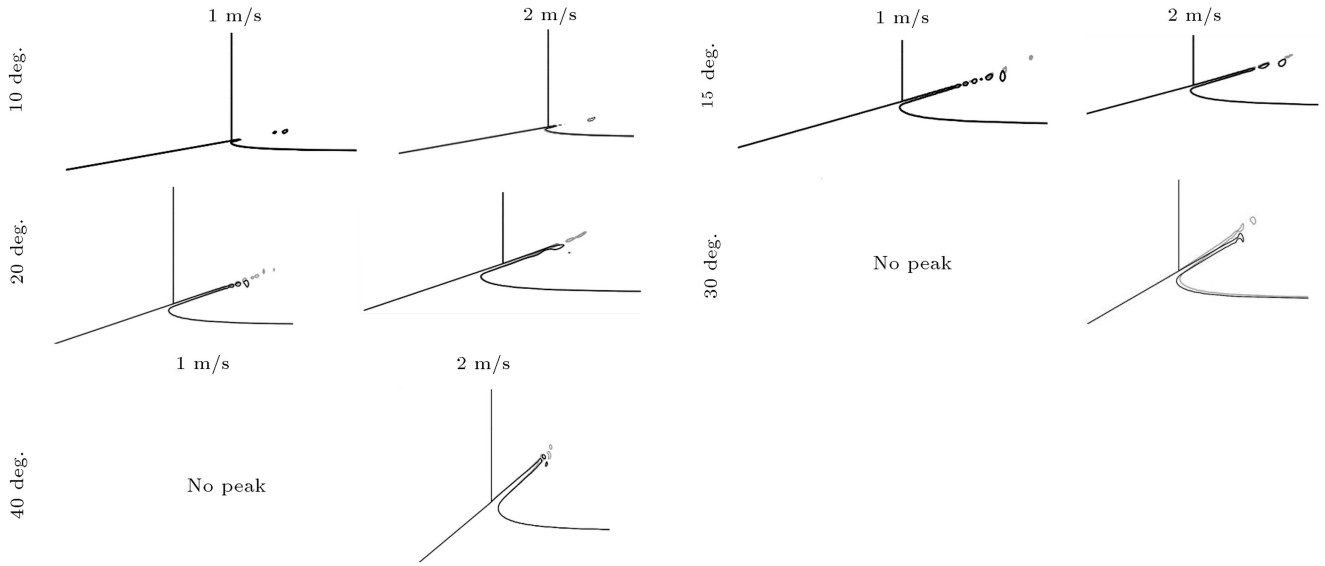

Figure 8. Free surfaces related to the peak force condition for different deadrise angles at different speeds in turbulent (black line) and laminar (gray line) simulations.

results due to the turbulence effect. In fact, turbulence causes the 2nd impact to occur 0.25 to 0.5 seconds sooner for all cases. Also, there is a 1.6% up to 66% augmentation in the 2nd impact force. However, the 66%, which corresponds to the 50 degrees case, cannot be taken into account, because the secondary impact in fact occurs in a non-ordinary manner, due to the high deadrise angle. Therefore, the highest difference in the secondary impact is assumed to occur at 40 degrees with a difference of 14.28%. It can therefore be concluded that the turbulence effect is significant in the secondary impact simulation.

The cavity formation at the "2nd impact" is illustrated in Figure 13.

As observed in Figure 13, contrary to the force estimation where there are large differences between laminar and turbulent simulations, the free surfaces are not so different.

4.4. Final intake of turbulent effect

In the previous sub-sections, the differences between laminar and turbulent flows were illustrated for three points of interest in the water entry problem. Maximum deviations of the laminar and turbulent flows in different points are illustrated in Figure 14.

As a conclusion about the effects of the turbulence on the water entry forces and free surfaces, it can be stated that there are no significant differences in the force and free surface estimations at the peak and hollow points. However, if the aim of a simulation is to analyze the secondary impact forces, special attention should then be paid to the turbulence or laminar assumptions. In recap, the turbulence affects the force estimation in the secondary impact, but has negligible effects on the main water impact. Therefore, it may be deduced that in many cases where the secondary impact is not needed, it is unnecessary to use any turbulence model. However, when the focus of the analysis is on the secondary impact, the use of a turbulence model is inevitable.

5. Conclusions

The aim of the present paper has been to examine the effects of turbulent and laminar flow assumptions on the water entry problem at different deadrise angles and velocities. To this end, finite element-based finite volume method (FEM-FVM) has been used to solve the governing Navier Stokes equations. This method has been coupled with Volume Of Fluid (VOF) scheme to simultaneously model the two phase flows. Furthermore, to model the turbulence effect, the $k-\varepsilon$ method has been implemented.

Wedges with deadrise angles ranging from 10 to 60 degrees have been simulated at two different velocities of 1 and 2 m/s with and without the turbulence assumption. Subsequently, by selecting three different critical instances of "peak", "hollow", and "2nd impact" in a typical impact force diagram, the forces and free surfaces have been extracted and differences between the turbulent and laminar simulations have been analyzed.

Based on the obtained results, it has been demonstrated that no significant difference is observed between the results of the critical instances of "peak" and "hollow" with errors less than 1.33% and 2.77%, respectively. Therefore, when studying the main impact in the water entry problem, the turbulence effect is negligible and there is no need to use any turbulence model. However, in the case of a secondary impact of the

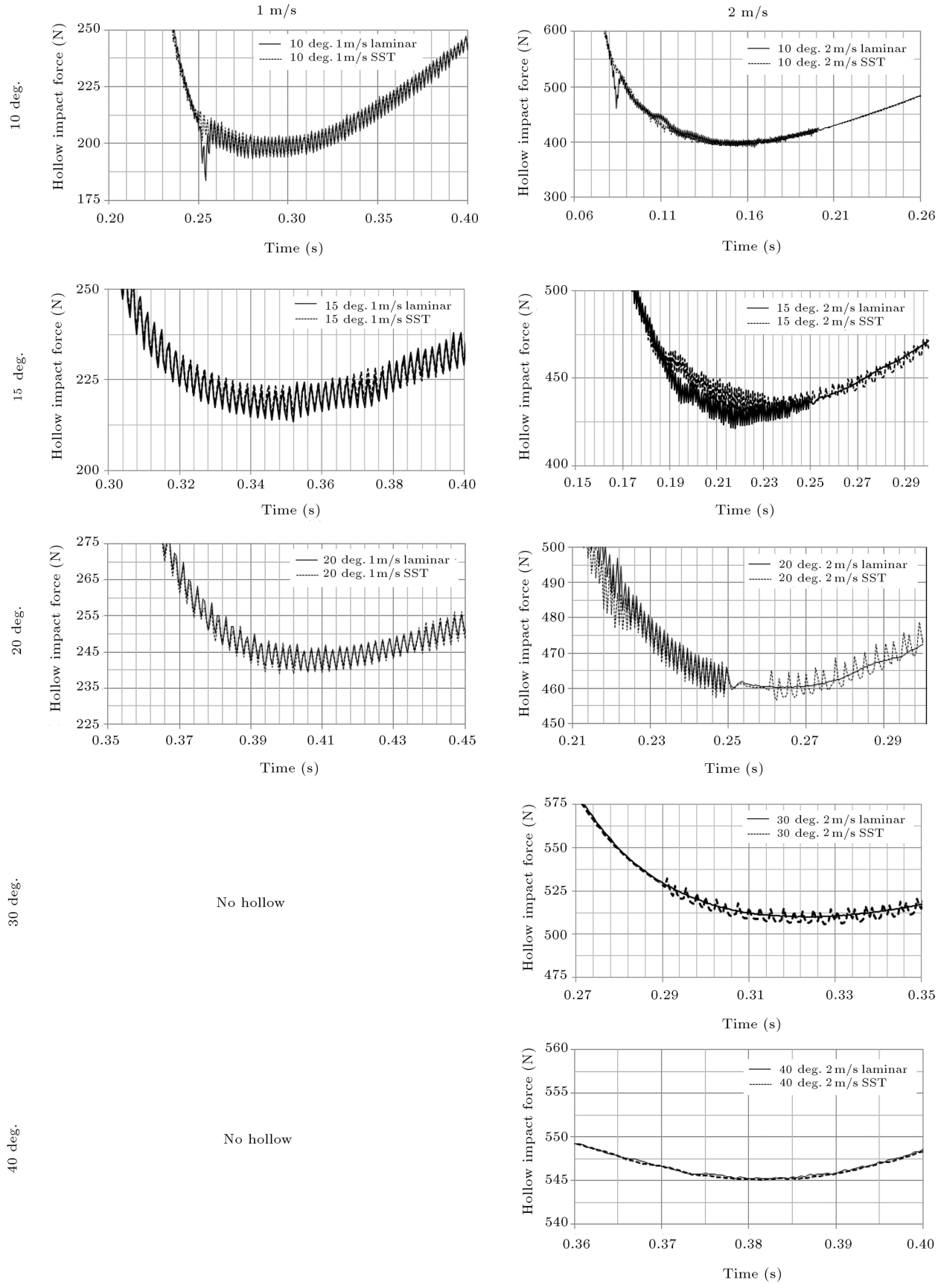

Figure 9. Impact forces acting on the wedges of different deadrise angles at different speeds in turbulent and laminar simulations in the hollow.

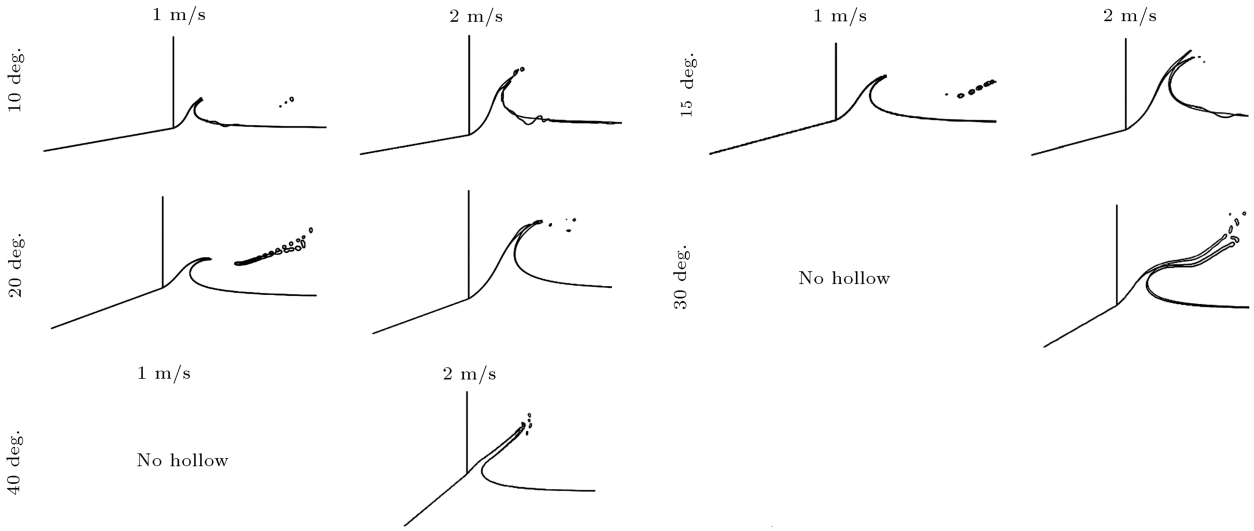

Figure 10. Free surfaces associated with the hollow point for different deadrise angles at different speeds in turbulent (black line) and laminar (gray line) simulations.

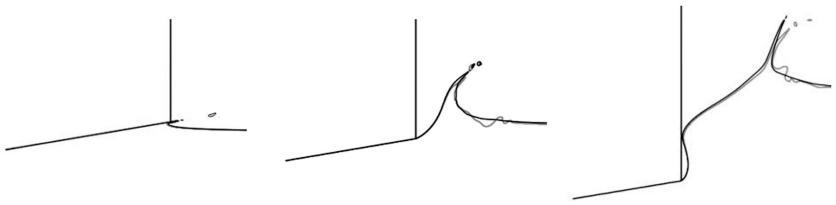

Figure 11. The secondary impact process.

wedge, it has been demonstrated that the effect of turbulence model can be up to 14.25%. This observation clearly shows the importance of the choice of turbulence model in analyzing the secondary impact of the wedges.

Overall, the present study has shown that it is unnecessary to use turbulence models for the main impact of the wedge, which is the main concern of many applications of this problem. However, to analyze the secondary impact, turbulence modeling becomes imperative in achieving better results.

Nomenclature

ρ	Density
μ	Molecular kinematic viscosity
u	Velocity in x direction
v	Velocity in y direction
ρ_1	First fluid density
ρ_2	Second fluid density
k	Turbulence kinetic energy
μ_t	Turbulence viscosity
P_k	Product of k
N	Shape function
j, k	Integration points
ds_y	Components of surface element in the y direction
φ_i^0	Parameter value at integral point in previous time step
$\overrightarrow{\hat{V}}$	Velocity vector in continuity equation in previous time step
τ	Shear stress
φ	Parametric value
S	Source term
α	Volume fraction
ds	Surface element
ρ_{eq}	Equivalent fluid density
υ_{eq}	Equivalent fluid density
ε	Specific dissipation rate
$C_{\varepsilon 1}, C_{\varepsilon 2}$	Closure coefficients and relations (constants).
$\sigma_\varepsilon, \sigma_k$ $P_{\varepsilon b}, P_{kb}$	Buoyancy effects
$\tilde{\forall}_i$	Sub-volumes in an element
ds_x	Components of surface element in the x direction
$\|_{j,k}$	Transformed integral forms at integration points
$\Delta t, \delta t$	Time step
p	Static pressure

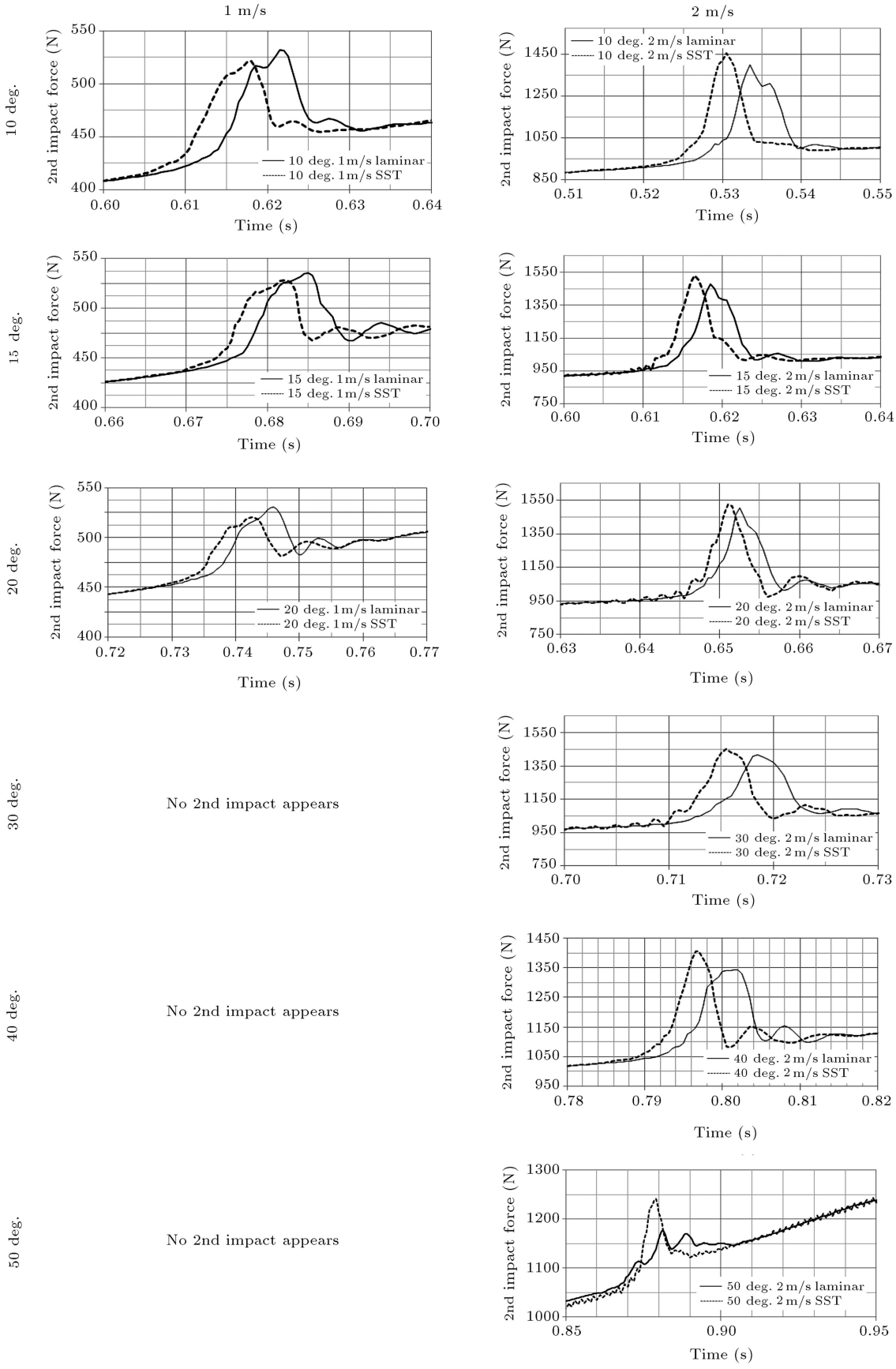

Figure 12. 2nd impact forces acting on wedges of different deadrise angles at different speeds in turbulent and laminar simulations.

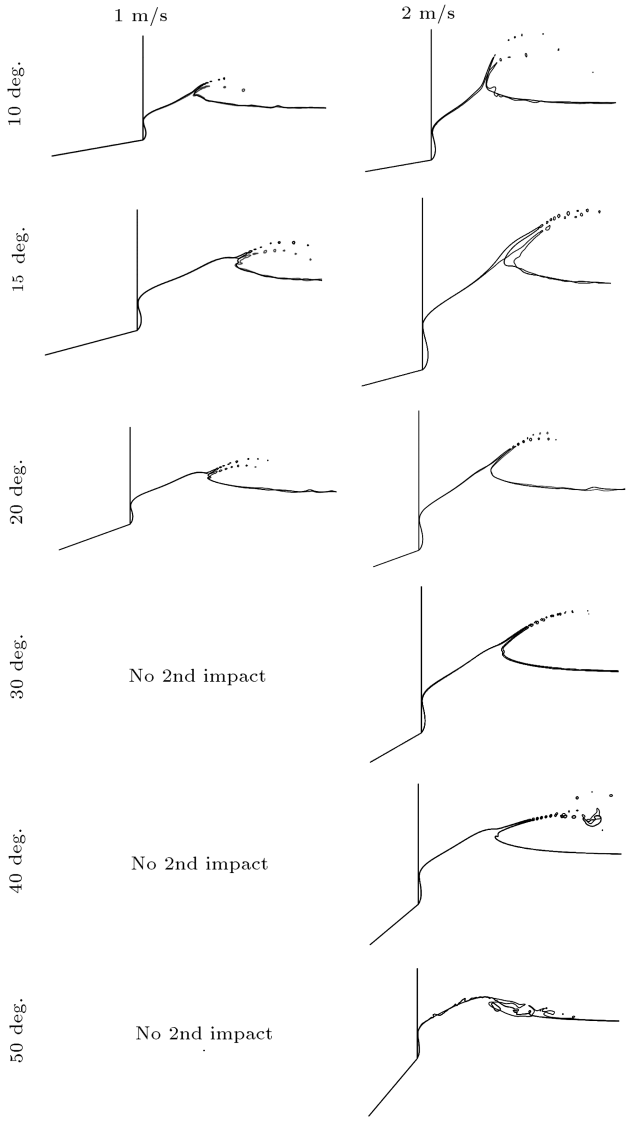

Figure 13. Free surfaces related to the 2nd impact for different deadrise angles at different speeds in turbulent (black line) and laminar (gray line) simulations.

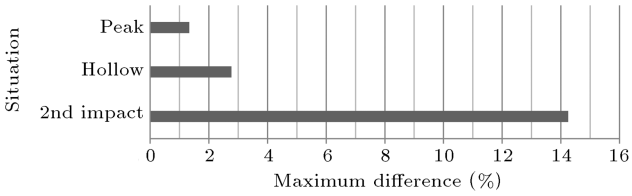

Figure 14. Maximum differences between the results of laminar and turbulent simulations.

References

1. Luo, H., Wang, H. and Soares, C.G. "Numerical prediction of slamming loads on a rigid wedge subjected to water entry using an explicit finite element method", *Advances in Marine Structures*, Guedes Soares & Fricke, Eds., pp. 41-48, CRC Press, New York, London (2011).
2. Yang, Q. and Qiu, W. "Numerical solution of 3-D water entry problems with a constrained interpolation profile method", *J. Offshore Mech. Arct. Eng.*, **134**(4), pp. 041101(1-8) (2012).
3. Gong, K., Wang, B. and Liu, H. "Modelling water entry of a wedge by multiphase SPH method", *32nd Int. Conf. on Coastal Eng.*, Shanghai, China, pp. wave. 10(1-10) (2010).
4. Gong, K., Liu, H. and Wang, B.l. "Water entry of a wedge based on SPH model with an improved boundary treatment", *J. of Hydro.*, **21**(6), pp. 750-757 (2009).
5. Shao, S. "Incompressible SPH simulation of water entry of a free-falling object", *Int. J. Numer. Meth. Fluids*, **59**(1), pp. 91-115 (2009).
6. Viviani, M., Brizzolara, S. and Savio, L. "Evaluation of slamming loads on a wedge-shaped section at different heel angles adopting SPH and RANSE methods", *12th Int. Cong. Int. Maritime Associ. Mediterranean (IMAM 2007)*, Varna, Bulgaria, pp. 107-114 (2007).
7. Wang, Y.H. and Wei, Z.Y. "Numerical analysis for water entry of wedges based on a complex variable boundary element method", *Explosion and Shock Waves*, **32**(1), pp. 55-60 (2012).
8. Yin, L. and Qian, Q. "Free water impacting analysis of a two-dimensional wedge", *J. Dalian Maritime Uni.*, **1**, pp. 96-100 (2010).
9. Sun, H., Zou, J., Zhuang, J. and Wang, Q. "The computation of water entry problem of prismatic planning vessels", *3rd International Workshop on Intelligent Systems and Applications (ISA)*, pp. 1-4 (2011).
10. Ghadimi, P., Saadatkhah, A. and Dashtimanesh, A. "Analytical solution of wedge water entry by using Schwartz-Christoffel conformal mapping", *Int. J. Model. Simul. Sci. Comput.*, **2**(3), pp. 337-354 (2011).
11. Gao, J., Wang, Y. and Chen, K. "Numerical simulation of the water entry of a wedge based on the complex variable boundary element method", *App. Mech. Materials*, **90-93**, pp. 2507-2510 (2011).
12. Wu, G.X., Xu, G.D. and Duan, W.Y. "A summary of water entry problem of a wedge based on the fully nonlinear velocity potential theory", *J. Hydro.*, **22**(5), pp. 859-864 (2010).
13. Khabakhpasheva, T.I. and Korobkin, A. "Elastic wedge impact onto a liquid surface: Wagner's solution and approximate models", *J. Fluids. Structs.*, **36**, pp. 32-49 (2013).
14. Yamada, Y., Takami, T. and Oka, M. "Numerical study on the slamming impact of wedge shaped obstacles considering fluid-structure interaction (FSI)", *22th Int. Offshore and Polar Eng. Conf.*, Rhodes, Greece, pp. 1008-1016 (2012).
15. Alaoui, A.E.M. and Neme, A. "Slamming load during vertical water entry at constant velocity", *22th Int. Offshore and Polar Eng. Conf.*, Rhodes, Greece, pp. 801-806 (2012).

16. Luo, H., Wang, H. and Soares, C.G. "Comparative study of hydroelastic impact for one free-drop wedge with stiffened panels by experimental and explicit finite element methods", *30th Int. Conf. on Offshore Mech. Arct. Eng. (OMAE)*, Rotterdam, Netherlands, pp. 119-127 (2011).

17. Yang, Q. and Qiu, W. "Numerical simulation of water impact for 2D and 3D bodies", *Ocean Eng.*, **43**, pp. 82-89 (2012).

18. Yang, Q. and Qiu, W. "Numerical solutions of 2D and 3D slamming problems", *Int. J. Maritime Eng.*, **153**(2), pp. A89-A97 (2011).

19. Yang, Q. and Qiu, W. "Computation of slamming forces on wedges of small deadrise angles using a CIP method", *18th Int. Offshore and Polar Eng. Conf.*, Vancouver, Canada, pp. 484-488 (2008).

20. Feizi Chekab, M.A., Ghadimi, P. and Farsi, M. "Investigation of three-dimensionality effects on aspect ratio on water impact of 3D objects using smoothed particle hydrodynamics method", *J. Brazilian Soc. Mech. Sci. Eng.*, **38**(7), pp. 1987-1998 (2016).

21. Ghadimi, P., Feizi Chekab, M.A. and Dashtimanesh, A. "Numerical simulation of water entry of different arbitrary bow sections", *J. Naval Archit. Marine Eng.*, **11**(2), pp. 117-129 (2014).

22. Ghadimi, P., Dashtimanesh, A. and Djeddi, S.R. "Study of water entry of circular cylinder by using analytical and numerical solutions", *J. Brazilian Society of Mech. Sci. Eng.*, **37**(3), pp. 821-835 (2012).

23. Farsi, M. and Ghadimi, P. "Finding the best combination of numerical schemes for 2D SPH simulation of wedge water entry for a wide range of deadrise angles", *Int. J. Naval Archit. Ocean Eng.*, **6**, pp. 638-651 (2014).

24. Farsi, M. and Ghadimi, P. "Effect of flat deck on catamaran water entry through smoothed particle hydrodynamics", Institution of Mechanical Engineering Part M: J. Engineering for the Maritime Environment (2014).

25. Farsi, M. and Ghadimi, P. "Simulation of 2D symmetry and asymmetry wedge water entry by smoothed particle hydrodynamics method", *J. Brazilian Society of Mech. Sci. Eng.*, **37**(3), pp. 821-835 (2015).

26. Rhie, C.M. and Chow, W.L. "Numerical study of the turbulent flow past an airfoil with trailing edge separation", *AIAA Journal*, **21**(11), pp. 1525-1532 (1983).

27. Karimian, S.M.H. and Schneider, G.E. "Pressure-based computational method for compressible and incompressible flows", *J. Thermo Phys. heat Trans.*, **8**(2), pp. 267-274 (1994).

28. Tveitnes, T., Fairlie-Clarke, A.C. and Varyani, K. "An experimental investigation into the constant velocity water entry of wedge-shaped sections", *Ocean Eng.*, **35**(14-15), pp. 1463-1478 (2008).

Biographies

Roya Shademani received her MSc degree in Ship Hydrodynamics from Amirkabir University of Technology in 2008. She was admitted to the PhD program at Amirkabir University of Technology in 2010 and is currently working on her dissertation. Her research interests include CFD analysis of hydrodynamic phenomena. She has co-authored 4 scientific papers in the field of computational fluid dynamics and hydrodynamics.

Parviz Ghadimi received his PhD in Mechanical Engineering in 1994 from Duke University, USA. He served one year as a Research Assistant Professor in M.E. and six years as a Visiting Assistant Professor in Mathematics Department at Duke. He is currently a Professor of Hydromechanics in Department of Marine Technology at Amirkabir University of Technology, Iran. His main research interests include hydrodynamics, hydro-acoustics, thermo-hydrodynamics, and CFD and he has authored over 80 scientific papers in these fields.